Journal of Power Sources 215 (2012) 266–273

Contents lists available at SciVerse ScienceDirect

Journal of Power Sources

journal homepage: www.elsevier.com/locate/jpowsour

Ex situ testing method to characterize cathode catalysts degradation under simulated start-up/shut-down conditions – A contribution to polymer electrolyte membrane fuel cell benchmarking

A. Marcu [a,*], G. Toth [a], S. Kundu [b], L.C. Colmenares [c,1], R.J. Behm [c]

[a] *Daimler AG, R&D MEA and Stack Technology, 73230 Kirchheim-Nabern, Germany*
[b] *Automotive Fuel Cell Cooperation, 9000 Glenlyon Parkway, Burnaby, BC V5J 5J8, Canada*
[c] *Institute of Surface Chemistry and Catalysis, Ulm University, D-89069 Ulm, Germany*

HIGHLIGHTS

- Start-up/shut-down test protocol development.
- Translation of the automotive stack voltage responses.
- Start-up/shut-down degradation mechanism.
- Evaluation methodologies for cathode catalysts.

ARTICLE INFO

Article history:
Received 21 December 2011
Received in revised form
18 April 2012
Accepted 6 May 2012
Available online 12 May 2012

Keywords:
Fuel cells
Electrochemical testing method
Start-up/shut-down
Degradation mechanism
Testing standard
Carbon corrosion

ABSTRACT

The paper introduces a novel *ex situ* test procedure that was developed to quantify the ageing of catalyst layers under critical automotive fuel cell conditions during start-up/shut-down phases. It is based on liquid electrolyte measurements, using a thin film catalyst electrode. The overall degradation under start-up/shut-down conditions is assessed by the decay in electrochemically active surface area. Furthermore, contributions from different processes leading to catalyst degradation such as Pt dissolution and Pt particle growth/agglomeration can be separated. Finally, using a differential electrochemical mass spectrometry (DEMS) set-up, also the extent and role of carbon corrosion under these conditions is accessible. The potential of this, compared to *in situ* fuel cell stack tests, rather fast and less costly *ex situ* test procedure is demonstrated in measurements using a commercial, graphitized carbon-supported Pt catalyst. The results of the degradation test and in particular the contributions from different degradation processes such as Pt dissolution, Pt particle growth/agglomeration and carbon corrosion during different stages of catalyst ageing are discussed.

1. Introduction

Proton Exchange Membrane Fuel Cells (PEM FCs), despite being a promising alternative to combustion engines, still face many challenges related to cost and durability. In order for automotive fuel cells to become commercially attractive, the current operational lifetime of 2500 h must be increased to 6500 h [1]. Over this lifetime, an automotive fuel cell will be exposed to over 13,600 start-up events and 500,000 short drive cycles [2], both of which are key drivers for degradation. Cathode catalyst degradation during transient operation causes a gradual decline in performance through the loss of the electrochemical surface area (ECSA) of platinum [3–9]. Considering that the cathode accounts for 55–77% of the total PEM FC stack cost [10–12], it is important to understand the mechanisms of the degradation processes that occur during automotive fuel cell operation. Of particular interest is the degradation during start-up and shut-down (SU/SD) events in a vehicle [13]. During shut-down, air will slowly fill the anode flow field of the fuel cell that initially was filled with hydrogen gas, causing a hydrogen/air front to move through the anode channels. Similarly, during start-up, hydrogen is fed to the anode, creating a H_2/air front. It has been found that the cathode voltage reaches potentials higher than 1.4 V, depending on the velocity of the H_2/air front

* Corresponding author. Tel.: +49 1748 710813; fax: +49 711 3052121269.
E-mail address: alina.marcu@web.de (A. Marcu).
[1] Present address: SINTEF Materials and Chemistry, New Energy Solutions, Sem Sælandsvei 12, N-7465 Trondheim, Norway.

0378-7753/$ – see front matter © 2012 Elsevier B.V. All rights reserved.
doi:10.1016/j.jpowsour.2012.05.010

filling the anode side of the system [13]. This creates a high interfacial potential difference in the region of the H_2/air interface, causing carbon corrosion and oxygen evolution at the cathode electrode. Catalyst degradation mechanisms under SU/SD conditions are often studied using the PEM FC stack as test object, by *in situ* test methods [13]. These tests, however, can be costly, they do not allow to discriminate between different processes contributing to the overall degradation [14,15], which prevents a deeper understanding of the specific mechanisms for catalyst degradation. The *in situ* tests often require larger amounts of catalyst material and therefore are not always suitable when assessing new research catalysts. In addition, in PEM FC the degradation is difficult to quantify and particularly the amount of dissolved Pt since it is trapped in the membrane and in the ionomer of the catalysts layer. For rapid evaluation of catalyst materials, model studies in liquid electrolyte (*ex situ* characterization) and accelerated degradation tests would be highly desirable. To be useful, the testing method must allow i) for a fast screening of different catalysts and ii) to distinguish between different degradation mechanisms, while being faster, more efficient and, most important, relevant to automotive operational modes. The US Department of Energy (USDoE) has provided two *ex situ* protocols to study catalyst degradation. One involves a potentiostatic hold test at 1.2 V; which it is used to assess the stability of the high surface area carbon support material, and the second one is a dynamic test used to evaluate the durability of the electrocatalytically active nanoparticles under load cycling. The latter consists of 30,000 square wave cycles (SWC) between idle and peak power conditions of 0.6/0.7–0.9/1.0 V [16–18]. The US Fuel Cell Council (USFCC) has also proposed a degradation test, consisting of 1000 SWC between 0.6 and 1.2 V, that is generally accepted for evaluating the electrocatalyst durability, and a 1.5 V potential hold test to examine the carbon support stability, especially of current state-of-the-art graphitized carbon support materials [16]. Though the protocols from the USDoE and USFCC separately evaluate the catalyst stability upon cycling and/or holding at high potentials, they do not properly simulate SU/SD events in a vehicle. Therefore, these tests may not provide as much insight into the specific degradation mechanisms characteristic for these applications. Several groups have suggested different *ex situ* cycling tests at potentials between 0.6 and 1.5 V [19,20] or between 0.85 and 1.5 V [21]. However, degradation tests studying start-up/shut-down cathode events separately and combined in a liquid electrolyte environment have not been reported so far.

In this work, we propose a potential cycling protocol which was developed from automotive stack voltage responses and which reproduces the main features exhibited during SU/SD processes. Combined electrochemical and mass spectrometric measurements in a differential electrochemical mass spectrometry (DEMS) set-up were employed to follow the degradation of the catalyst during potential cycling with time. The SU/SD degradation process is analyzed to identify which parts of the SU/SD cycle contribute most to degradation. Finally, the physical changes of the catalyst caused by SU/SD cycling are characterized. The results provide a solid basis for an application relevant evaluation of the cathode catalyst durability and degradation under SU/SD operating conditions.

2. Experimental

2.1. Electrochemical and DEMS measurements

The electrochemical and mass spectrometric measurements were performed in a dual thin-layer flow-through DEMS cell, which was connected to a differentially pumped vacuum chamber system with a Pfeiffer Vacuum quadrupole mass spectrometer (QM 422) [22–25]. Potential control was achieved with a potentiostat from Solatron (Analytical Multistat 1480). A thin film of catalyst supported on a glassy carbon stub, was used as working electrode. Two Pt wires served as counter electrodes and a saturated calomel electrode was used as reference electrode. All potentials are referenced against that of a reversible hydrogen electrode RHE. The degradation measurements were conducted in 0.5 M H_2SO_4 electrolyte under controlled flow, with the electrolyte continuously purged with argon. All DEMS experiments were reproduced by rotating ring disk electrodes (RDE) as well, showing similar ECSA degradation behavior as in DEMS.

2.2. Thin film catalyst electrode preparation

Using a commercial graphitized carbon-supported Pt catalyst, a catalyst ink consisting of 2 mg catalyst per cm^3 aqueous solution was prepared. The suspension was ultrasonicated for 30 min at room temperature before a 25 μl aliquot was dispersed onto a mirror polished glassy carbon disk from Sigradur GmbH Germany of 9 mm diameter and then dried under nitrogen. An aqueous Nafion solution was then added following the method proposed by Schmidt et al. [26]. It was shown that the diffusion resistance of the Nafion film is negligible due to its low thickness [26]. The working electrode was transferred to a thin-layer flow-cell. Prior to the electrochemical measurements, the catalysts was electrochemically cleaned by sweeping the potential between 0.06 and 1.2 V, until a steady voltammogram was obtained.

2.3. ECSA loss determination

The platinum ECSA of each catalyst sample was determined using the mean integral charge of the hydrogen adsorption areas, obtained at 10 mV s^{-1} and room temperature, considering a charge of 210 μC $cm_{Pt}{}^{-2}$ for a full monolayer (ML) of H_{upd} and assuming a H_{upd} coverage of 0.77 ML at the onset of hydrogen evolution [22,27]. Each of the accelerated events included 1000 potential cycles, stopping after 100, 200, 400, 600, 800, 1000 cycles in order to determine the ECSA and the cumulative carbon mass via the CO_2 signal (see below).

2.4. Carbon corrosion

The carbon mass loss was quantified by measuring the CO_2 evolution during the different potential cycle tests in a DEMS set-up. This allows simultaneous measurements of the Faradaic current at a thin film working electrode and online measurements of the carbon corrosion via the resulting CO_2 evolution. Gaseous products such as CO_2 diffuse from the working electrode through a porous membrane to a mass spectrometer; the membrane is provided by Scimat® and has 50% porosity, a thickness of 60 μm and 0.2 μm pore diameter. The mass signal of CO_2 ($m/z = 44$) recorded during potential cycling is then used to determine the carbon weight loss m_{carb} via the following relation:

$$m_{carb} = (A_w \cdot Q_{CO_2}) \Big/ \left(F \cdot K^*\right) \quad (1)$$

where A_w is the atomic weight of carbon ($A_w = 12.01$ g mol^{-1}); Q_{CO_2} is the charge of the mass spectrometric CO_2 signal ($mz^{-1} = 44$); F is the Faraday constant ($F = 96{,}485$ C mol^{-1}) and K^* the calibration constant of the CO_2 signal. The calibration constant K^*, which allows to calculate the number of CO_2 molecules from the charge in the mass spectrometric CO_2 signal and which is defined by [22]:

$$K^* = \frac{z \cdot Q'_{CO_2}}{Q_F} \quad (2)$$

was measured during oxidation of pre-adsorbed CO (CO_{ad} stripping'). Q'_{CO_2} and Q_F are the mass spectrometric ($mz^{-1} = 44$) and the Faradaic charges, respectively, and z is the number of electrons released per adsorbed CO molecule which is oxidized to CO_2. For the calibration procedure, CO_{ad} stripping was performed by first adsorbing CO at a constant electrode potential of 0.06 V for 10 min, by injecting 2 ml of CO saturated 0.5 M H_2SO_4 solution. After CO adsorption, the cell was carefully flushed with Ar saturated electrolyte at the same electrode potential in order to remove the excess of dissolved CO. The CO_{ad} layer was oxidatively stripped in a potential scan (scan rate 10 mV s^{-1}), starting from the adsorption potential and recording both Faradaic and $mz^{-1} = 44$ ion current.

To ensure that during high potentials the CO_2 signal results only from the sample and not from oxidation of the glassy carbon support, a blank experiment was conducted using a catalyst free glassy carbon electrode.

2.5. Elemental and structural analysis

One of the advantages of the flow-cell system is the ability to collect the electrolyte in which platinum was dissolved during the degradation tests. The amount of dissolved platinum from the working electrode in to the electrolyte was determined by elemental analysis by Inductively Coupled Plasma Mass Spectroscopy (ICP-MS) with a platinum detection limit of 0.001 mg l^{-1}. The electrolyte (flow of 20 μl s^{-1}) was collected continuously and removed after 0, 100, 200, 400, 600, 800, 1000 cycles for Pt content analysis.

Transmission electron microscopy (TEM) images were obtained using a JEOL 3010 microscope operated at 300 kV. Particle size and size distribution was evaluated before and after the electrochemical measurement, using the particle analysis function of the Digital Micrograph software Gatan, by counting 500 particles.

3. Results and discussion

Depending on the fuel cell application, the cathode catalyst may be exposed to various potential windows. Typically, the fuel cell cathode is operated at voltages between 0.6 and 0.9 V [28] during a normal drive cycle. When the car is turned off, air ingress into the fuel cell anode creates an air/air condition, where the measured potential of both electrodes is about 1.0 V [13]. During SU/SD, the potential experienced by the cathode catalyst can be higher than 1.4 V [19,29,30] for short periods of time.

3.1. SU/SD degradation test

During fuel cell SU/SD, the H_2/air flow developed on the anode side leads to cathode potentials that cause accelerated degradation of the electrocatalysts [29,30]. In order to follow the voltage behavior with the change in the H_2/air flow, Fig. 1 displays the voltage trace collected from *in situ* measurements. The plot was generated by measuring half cell potentials, using a proprietary reference electrode. Loop currents were generated by flowing air continuously on the cathode while the anode gas was switched between air and hydrogen. When air is flowing through both electrodes, anode and cathode, a rest potential of 1.04 V is measured. Once hydrogen is flushed over the air at the anode side, the surface Pt oxides are reduced and the anode potential drops gradually to 0 V. On the cathode side, the potential rises to 1.45 V, further oxidizing Pt and carbon in response to the lack of protons and electrons from the anode, damaging the cathode catalyst layer. Afterward, the anode filled with H_2 has a potential of 0 V and the cathode filled with air has a potential of 0.9 V.

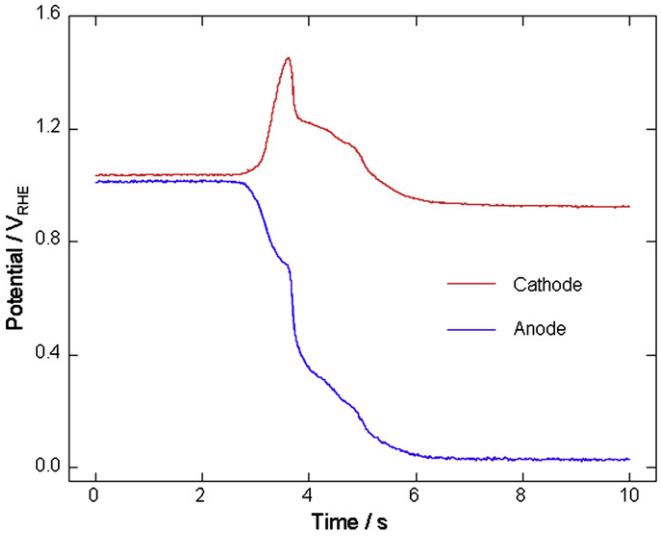

Fig. 1. Voltage profile of cathode and anode for a Pt/C electrode on a MEA, under SU/SD conditions, originating from air/air conditions on both sides.

The *in situ* SU/SD voltage behavior illustrated in Fig. 1 was used to develop an *ex situ* SU/SD degradation test for fast and reliable testing of the electrocatalyst durability. The development of a combined, accelerated cathode SU/SD testing protocol in a liquid electrolyte environment allowing to identify the contributions of the different degradation processes responsible for the loss in ECSA has not been reported so far. Cycle A in Fig. 2 illustrates a potential cycle which summarizes both events SU and SD on the cathode side of a PEM FC. The cycle begins with the SD event, which is simulated by varying the potential from normal driving (0.6 V) to peak (1.4 V) conditions and holding the upper potential for 30 s. Afterward, the potential is fixed at 1.0 V for 30 s to simulate the condition when the car is resting and is filled with air. In order to mimic the start-up event, the potential is again increased from 1.0 V to 1.4 V for 30 s, followed by a return to the normal driving voltage of 0.6 V for 30 s. The above SU/SD profile was analyzed to determine which portion of the profile contributes most to the overall cathode degradation. Each SU/SD cycle includes at least three different potential steps

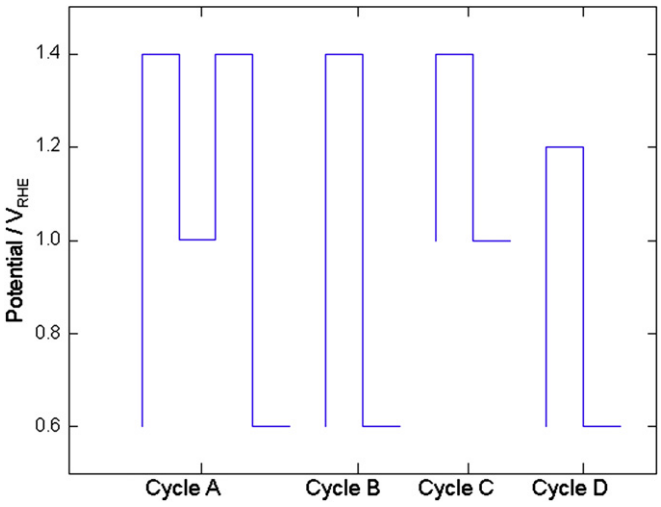

Fig. 2. Profiles of square wave cycles for accelerated durability measurements: A represents the SU/SD profile of 0.6–1.4–1.0–1.4–0.6 V; B represents the large voltage window 0.6–1.4 V in A; C represents the narrow voltage interval 1.0–1.4 V in A; D the reference test 0.6–1.2 V.

from 0.6 V to 1.4 V to 1.0 V for the shut-down portion and from 1.0 V to 1.4 V to 0.6 V for the start-up event. Therefore, two separate model protocols were studied: cycle B, which separates the wide cycling window from 0.6 to 1.4 V at the start and end of the SU/SD cycle, and cycle C, that isolates the narrow cycle window between 1.0 and 1.4 V. In addition to the above protocols, the USFCC [16] cycling protocol, which consists of square wave cycling (SWC) between 0.6 and 1.2 V, was considered as well for comparative purposes. There are several ways to mitigate the H_2/air front related voltage. Nevertheless, since currently the fuel cell stack voltage definitely does exceed 0.9 V in start-up/shut-down and H_2 starvation situations, we find the high potentials used in the present work realistic to mimic the long term behavior a stack is exposed to and the related degradation. In the following, the analysis of the Pt and carbon support stability under the proposed testing protocol conditions is described, and we identify and quantify the structural changes of the catalyst induced by SU/SD cycling.

3.2. Platinum surface area loss

Fig. 3 shows the ECSA loss resulting during the four different potential cycling profiles. The error bars are based on the values obtained in a single DEMS measurement and two measurements using a rotating ring disk electrode (RRDE) on two catalysts samples. In all cases, the ECSA of the catalyst decreases with increasing cumulative number of cycles, the upper potential limit (cycle B vs. cycle D) and the potential window range (cycle B vs. cycle C and vs. cycle D). Each SU/SD cycle is comprised of one cycle from 0.6 to 1.4 V illustrated in Fig. 2 (cycle B) and one cycle from 1.0 to 1.4 V illustrated as cycle C in Fig. 2. A sequence of 1000 cycles B led to a cumulative ECSA loss of 76%, while a similar sequence of C type cycles caused a loss of 18% (Fig. 3). The two cycles together result in a similar cumulative ECSA loss as obtained in the overall SU/SD testing protocol of cycle A (94%). The result shows that the portion of the SU/SD cycle involving the largest change of the potential contributes most to the overall catalyst degradation as measured by the decrease in ECSA. Comparing cycling along protocol B with that using protocol C, the ECSA loss was 50% higher for B than for C. It is known that high potentials such as 1.4 V result in the formation of platinum surface oxides on the Pt nanoparticles, and potentials around 1.0 V are not low enough to completely reduce these oxides. Therefore, the degradation process is hindered and the electrochemically active Pt surface is largely passivated, as seen in cycle C. However, when the potential is lowered to 0.6 V, the oxide layer is largely reduced, which leads to an increased platinum dissolution when the potential is stepped back to high values (1.4 V). This behavior is found in cycle B, in agreement with literature data [31–33].

The effect of potential cycling in the range of 0.6–1.2 V in cycle D resulted in a 52% platinum ECSA loss, which is 20% less than that in cycle B (Fig. 3). This result is attributed to the increase of the upper potential from 1.2 V in cycle D to 1.4 V in cycle B. In general, the corrosion of the carbon-supported Pt catalyst is accelerated at potentials as high as 1.4 V. Since the time spent at high potentials varied considerably in the different cycles, we plotted the ECSA losses against the time spent at potentials higher than 1.0 V in Fig. 4. In the case of cycle A the time spent at high potentials is 90 s per cycle, which is longer than for cycles B and C with 30 and 60 s, respectively, spent at high potentials. After about 8 h cycling along the respective protocols (see Fig. 4), illustrated by the dotted line in Fig. 4, protocol B was found to be most corrosive, followed by A, D and finally C. Therefore, the fact that the highest degradation is observed during cycle A when plotting vs. the cumulative number of cycles (Fig. 3), is mainly due to the longer times spent at higher potentials in that protocol. Hence, the addition of cycle C to cycle B, which creates a profile identical to that of cycle A (Fig. 2), leads to a lower ECSA loss compared to that during B cycling, and thus to a stabilization of the catalyst. As discussed before, cycle A represents more properly the potential conditions encountered in the car during SU/SD, and thus is more suitable to investigate cathode catalyst materials under conditions close to SU/SD events encountered in fuel cells.

3.3. Carbon mass loss

Another factor contributing to the degradation of the cathode catalyst is the corrosion of the carbon support material. Possible mechanisms of the carbon corrosion process have been discussed in the literature [15,19,21,30,34]. Therefore, the focus of this study was to quantify the carbon mass loss during the different potential cycles A, B, C and D. Fig. 5 shows the cumulative carbon weight loss, determined from the mass spectrometric CO_2^+ signal

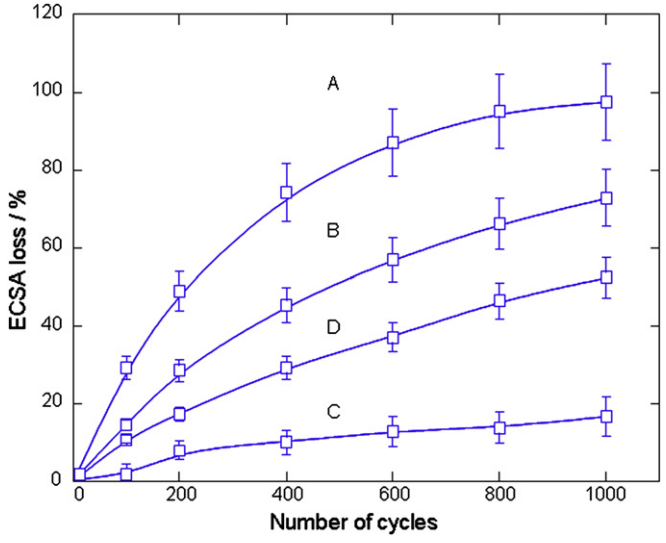

Fig. 3. Effect of the potential window on the Pt ECSA for increasing cycle number: A (0.6–1.4–1.0–1.4–0.6 V); B (0.6–1.4 V); C (1.0–1.4 V); D (0.6–1.2 V); 30 s each potential step.

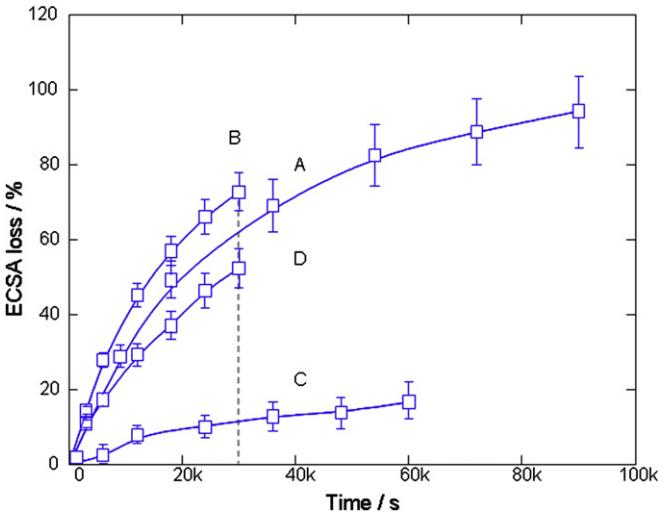

Fig. 4. Effect of the potential window on the Pt ECSA for increasing time spent at high potentials (above 1.0 V): A (0.6–1.4–1.0–1.4–0.6 V); B (0.6–1.4 V); C (1.0–1.4 V); D (0.6–1.2 V); 30 s each potential step.

($mz^{-1} = 44$) recorded simultaneously to the Faradaic current, as a function of the cumulative number of cycles. It shows very low cumulative carbon mass losses, with 6% in maximum obtained for cycle A (see Fig. 5). The error bars are based on DEMS measurements performed for two catalyst samples with graphitized carbon support (1 measurement per sample). The corrosion resistance of the carbon may be related to the graphitic nature of the carbon surface. Nevertheless, the (local) loss of carbon may severely weaken the interaction between Pt nanoparticles and the carbon support, and thus cause a detachment of the Pt nanoparticles from the support, resulting in a loss of ECSA. Carbon corrosion is highest during testing cycle A, followed by B and D, and it is lowest after cycling protocol C as illustrated in Fig. 5. When cycling between 0.6 and 1.4 V (cycle B), the carbon mass loss is 50% higher than during cycling in the potential window of 0.6–1.2 V (cycle D) and 70% higher than in the range of 1.0–1.4 V (cycle C). These experiments indicate that similar to the ECSA loss the carbon weight loss is approximately additive, as the added carbon losses for cycles B and C are comparable to those obtained during cycles A, despite the rather different cumulative times at potentials higher than 1.0 V.

Fig. 6 shows the carbon weight loss as a function of time spent at high potentials ($E > 1.0$ V). It is interesting to note that the carbon mass losses in D and C are similar after 8 h cycling, if only the time above 1.0 V is considered. Similar behavior was observed also for the ECSA loss (see above). Most likely, potentials of 1.2 V are not high enough to induce substantial carbon corrosion on graphitized carbon materials, and upon cycling in the potential window of 1.0–1.4 V corrosion is hindered by surface oxide species [21]. Decreasing the lower potential limit to 0.6 V in cycle B, carbon corrosion increases by a factor of four, from ~0.5%–~2.5%, compared with D and C. The combination of the potential cycles of B and C in the new SU/SD testing protocol A shows the influence of the strong passivation effect of the 'oxide' layer on the carbon support surface. The passivation effect imposed by the addition of cycle C into the protocol B is much more pronounced for carbon corrosion than for the platinum ECSA loss (see Fig. 4), comparing similar times spent at high potentials (30,000 s). Carbon corrosion is essentially reduced to half when cycles B and cycles A are compared, while the ECSA loss is only ~10% lower. This difference must be related to the specific degradation mechanism

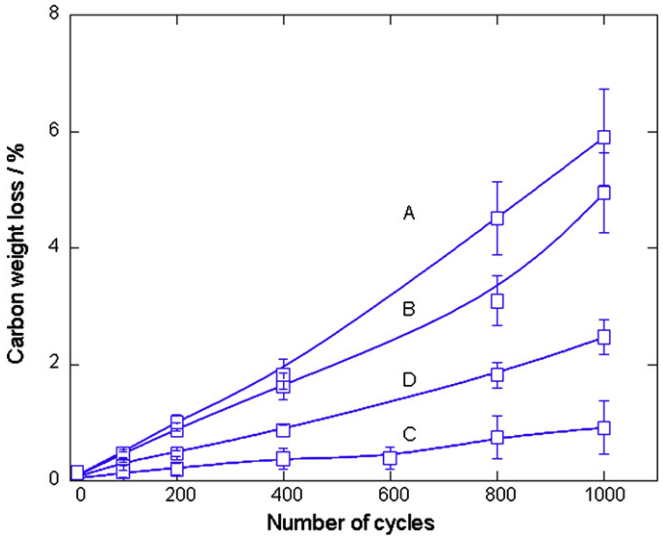

Fig. 5. Effect of potential cycling on the carbon weight loss for increasing number of cycles: A (0.6–1.4–1.0–1.4–0.6 V); B (0.6–1.4 V); C (1.0–1.4 V); D (0.6–1.2 V); 30 s each potential step.

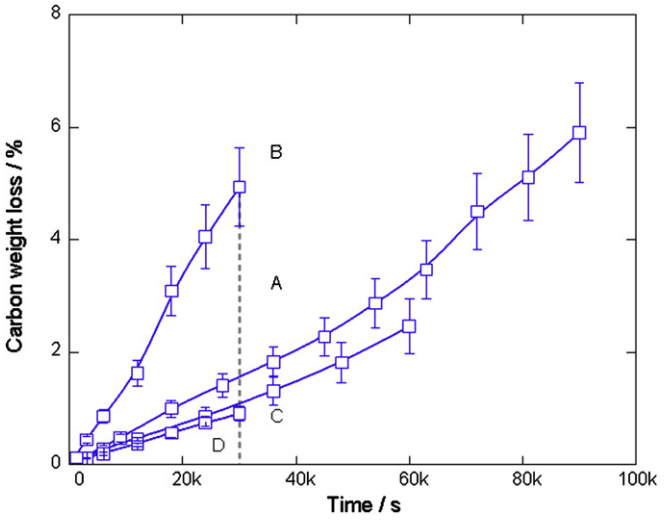

Fig. 6. Effect of potential cycling on the carbon weight loss for increasing time at high potentials: A (0.6–1.4–1.0–1.4–0.6 V); B (0.6–1.4 V); C (1.0–1.4 V); D (0.6–1.2 V); 30 s each potential step.

that dominates the losses of carbon and of Pt surface area at high potentials. Obviously, the passivation introduced by the narrow potential windows (1.0–1.4 V) is more efficient for stabilizing the ECSA against losses in the subsequent wide potential window (0.6–1.4 V) than for stabilization of carbon against surface oxidation. This may be related to the accelerated corrosion of carbon in the presence of Pt nanoparticles [29].

3.4. Separation of the different contributions to catalyst degradation

Several mechanisms are commonly held responsible for the loss of Pt ECSA such as Pt dissolution, Pt agglomeration and carbon corrosion [35–38]. To unravel which process has the biggest impact on the overall Pt ECSA losses, we tried to quantify the contributions from the individual degradation processes in the SU/SD durability test A. During the degradation, the liquid electrolyte was periodically collected and analyzed by ICP-MS in order to quantify the platinum mass loss. The Pt particle size was determined by TEM analysis at the beginning and at the end of the test. The contribution from carbon corrosion was discussed already in Section 3.3. From TEM images, the volume–area mean particle size d_{va} of the fresh Pt/C catalyst was determined to 5.35 ± 0.45 nm (see Fig. 7). Assuming spherical particles, this mean particle size corresponds to a theoretical surface area $SA_T = 52.36 \pm 4.40\ m^2\ g_{Pt}^{-1}$, which is in good agreement with the experimental surface area $SA_E = 52.04 \pm 0.76\ m^2 g_{Pt}^{-1}$ determined by integration of the H_{upd} adsorption charge. After the SU/SD cycles (1000 cycles), there was a substantial change in particle shapes/sizes and in the distribution of platinum particles due to growth and agglomeration, and different particle shapes, both spherical and non-spherical shapes, could be distinguished, as illustrated in the TEM image in Fig. 7b. TEM images of the highly degraded catalysts are difficult to evaluate due to the large fraction of agglomerated and overlapping particles [39–41], which causes large deviations in the particle size distribution and in the calculation of the mean particle size. In order to not only rely on the TEM images, we also calculated the dispersion of the catalyst from electrochemical (H_{upd}) and analytical (ICP-MS) measurements. The catalyst dispersion can be considered as a parameter that provides information about particle growth/agglomeration and its relationship to ECSA loss. The

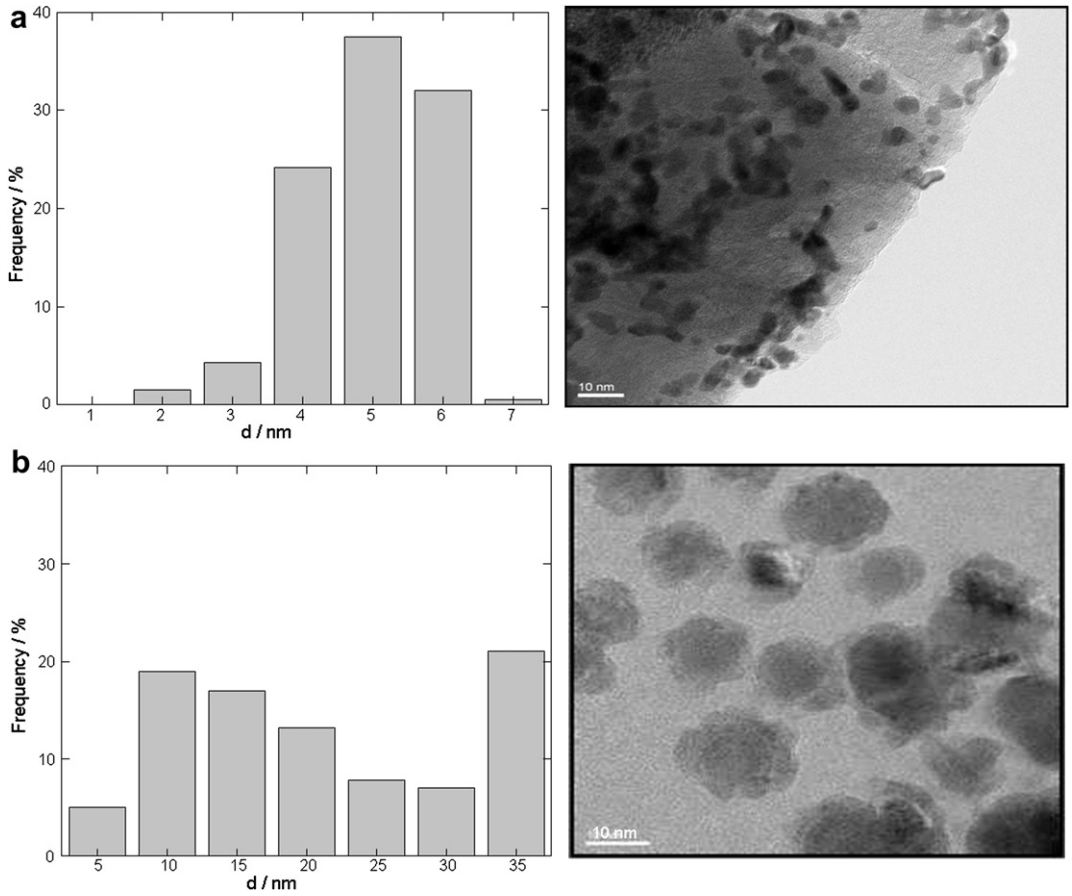

Fig. 7. TEM images of the Pt/C catalyst (a) before and (b) after the 1000 degradation cycling test using protocol A (0.6–1.4–1.0–1.4–0.6 V); 30 s each potential step.

dispersion is given by the ratio of the active Pt surface atoms and the total number of Pt atoms at the working electrode, as follows:

$$D_E = \frac{A_{Pt}}{T_{Pt}} \quad (3)$$

where: D_E is the dispersion of Pt particles, determined from experimental data, T_{Pt} is the total number of Pt atoms present at the working electrode, determined from the difference between the initial Pt loading and the Pt loss, during degradation cycles, measured by ICP (see Table 1) and A_{Pt} is the number of active surface platinum atoms, determined via the following relationship:

$$A_{Pt} = \left(\frac{Q_{H_{upd}}}{F}\right) * N_A \quad (4)$$

Table 1
ECSA, remaining Pt mass, active Pt mass and calculated dispersion as a function of number of cycles.

Cumulative no. SWCs	ECSAcm^{-2}	Remaining Pt mass[a]μg^{-1}	Active Pt mass[b]μg^{-1}	Dispersion/%
0	8.96	16.65	2.93	17.59
100	6.45	12.67	2.11	16.64
200	4.48	9.88	1.46	14.83
400	1.92	7.24	0.63	8.68
600	0.81	5.73	0.26	4.62
800	0.35	5.03	0.11	2.27
1000	0.11	4.51	0.04	0.82

[a] Determined from ICP-MS analysis.
[b] Determined from electrochemical data (H_{upd}).

where: $Q_{H_{upd}}$ is the hydrogen underpotential deposition charge (C), which is determined by integrating the hydrogen adsorption area of the measured basic voltammogram, F is the Faraday constant (F = 96,485 C mol^{-1}) and N_A is the Avogadro constant 6.02×10^{23} mol^{-1}.

For the fresh catalyst, the dispersion of $D_E = 0.17$ (see Table 1) calculated by this approach is in good agreement with the initial dispersion determined from the TEM data ($D_{TEM} = 0.17 \pm 0.014$). The above procedure is of great advantage since it does not rely on assumptions on the shape of the particles, in contrary to the TEM data, making it more accurate for characterizing fresh and, more important, degraded electrocatalysts. At the end of the degradation cycle A, the dispersion had decreased to $D_E = 0.0082$, and the corresponding surface area to $SA_E = 2.51$ $m^2 g_{Pt}^{-1}$.

In the following, we evaluate the quantitative contributions of the different degradation processes, Pt dissolution and Pt particle growth/agglomeration, to the ECSA loss. Fig. 8 shows the cumulative decay of the ECSA, of the amount of platinum (platinum dissolution) and of the dispersion from the fresh catalyst up to 1000 cycles of the SU/SD testing protocol (cycle A). The data indicate an exponential decay of the ECSA to a very low value of 2% of the initial value. Likewise, also the Pt mass decays about exponentially, but with a significantly higher final value (27% of the initial mass). In good agreement with these findings, the loss in dispersion is initially, in the first 200 cycles, rather small, but then increases significantly and exceeds that caused by Pt dissolution after about 500 cycles. Finally, also the dispersion has decayed to a very low value, about 5% of the initial value. Accordingly, the degradation of the catalyst is initially dominated by the dissolution of Pt. This

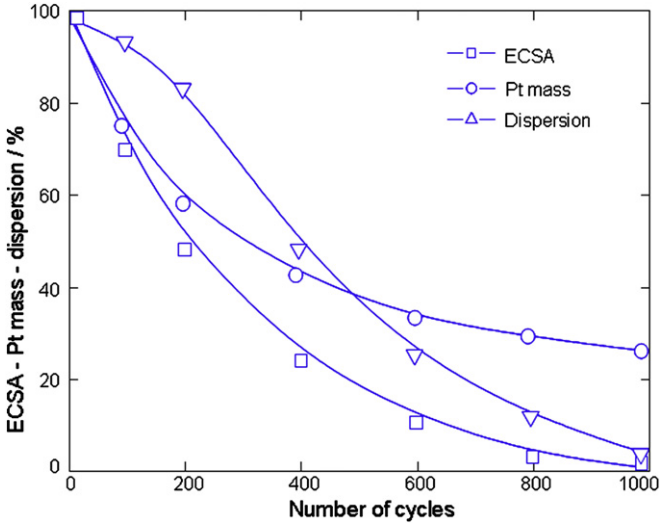

Fig. 8. Separation of the contributions from the different degradation processes – the cumulative decay of the ECSA, the Pt mass (Pt dissolution) and of the dispersion during cycling using protocol A (0.6–1.4–1.0–1.4–0.6 V) vs. the number of cycles.

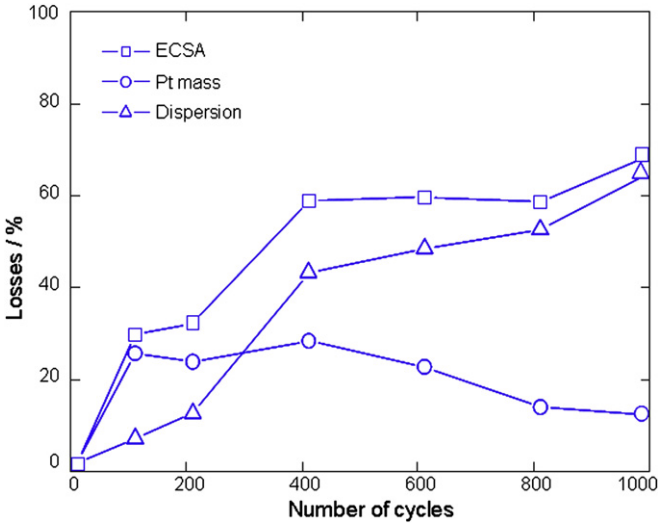

Fig. 10. Evolution of the overall ECSA loss and the losses due to Pt dissolution and Pt particle growth/agglomeration (dispersion) with increasing number of cycles using protocol A (0.6–1.4–1.0–1.4–0.6 V) (in all cases differential losses, see Table 1 for absolute values) (based on the measurements presented in Fig. 8).

process becomes less dominant after about 200 cycles, when the Pt particle increase leads to a steep decay of the dispersion, and finally growth/agglomeration of Pt particles, as indicated by the decay of the dispersion, is the dominant factor for the decay in ECSA.

The contributions of the two individual degradation processes, Pt dissolution and Pt particle growth/agglomeration, to the overall decay of the ECSA are more obvious from plots of the ECSA as a function of loss in Pt mass (Pt dissolution) and Pt dispersion (Pt particle growth/agglomeration), respectively, in Fig. 9. This plot reveals that the ECSA decreases linearly with the loss of platinum mass and about exponentially with the decrease of the dispersion, induced by the growth/agglomeration of the Pt particles. In the former case it is interesting to note that the ECSA is almost completely lost at a point (after 1000 cycles), where the Pt mass loss is about 73%. Hence, most of the remaining Pt mass of 4.5 μg at the working electrode (Table 1) must be agglomerated and essentially inactive. The large effective Pt particle size is reflected also by the very low final dispersion of only $D_E = 0.0082$, which is

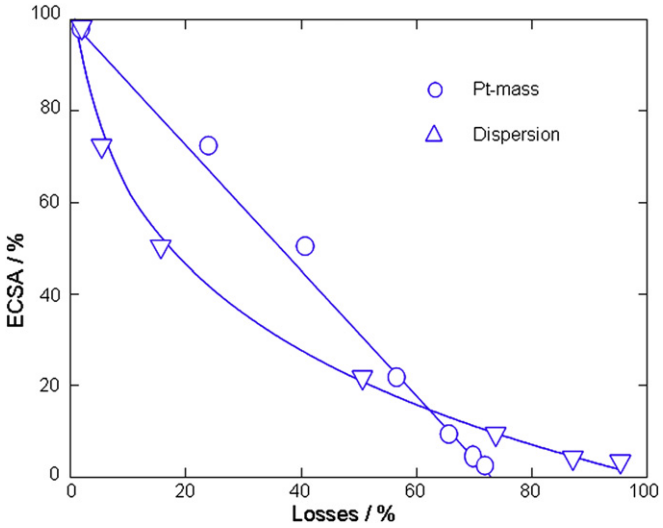

Fig. 9. The dependence of the ECSA on the cumulative loss of Pt mass and of the Pt dispersion, during cycling using protocol A (0.6–1.4–1.0–1.4–0.6 V) (based on the measurements presented in Fig. 8).

equivalent to a mean particle size of 100 nm, assuming spherical particles.

Further information on the contributions of the different degradation processes to the surface area loss during SU/SD degradation tests can be obtained from the differential losses of ECSA, Pt mass and dispersion, reflecting the relative change of these properties between subsequent analysis steps. These are plotted in Fig. 10 vs. the number of cycles (see also Table 1 for absolute numbers). For the first 100 cycles, the trace of the ECSA loss closely resembles that for Pt dissolution, indicating that the ECSA loss is mainly caused by irreversible Pt dissolution into the electrolyte. For the next 100 cycles, the losses in ECSA and Pt mass remain almost constant, while the dispersion loss increases, as expected for a beginning contribution from Pt particle growth/agglomeration to the overall ECSA loss. With further increasing number of cycles, up to 400 cycles, both ECSA loss and dispersion loss increase considerably, while Pt dissolution remains about constant. Hence, the contribution of Pt dissolution to the overall ECSA loss decreased significantly. Continuing stepwise to 1000 cycles, the increase in ECSA and dispersion losses continues, though less pronounced, while Pt dissolution decreases slightly. In combination, this results in a further decreasing contribution of Pt dissolution to the overall ECSA loss. Therefore, at the end of the SU/SD test, the ECSA loss is dominated by Pt particle growth/agglomeration; Pt dissolution still occurs, but at a lower rate. The decreasing contribution from Pt dissolution with continuing cycling agrees well with previous findings that platinum particle growth stabilizes them against dissolution [42].

4. Conclusions

A new *ex situ* catalyst durability test, assessing the catalyst stability and degradation processes under SU/SD conditions, has been developed as a practical and meaningful approach for benchmarking potential fuel cell catalysts. These *ex situ* tests have the advantage of being faster and less costly than *in situ* tests, and also avoid contributions from other components inside a fuel cell stack. The testing procedure allows us to distinguish between different degradation processes occurring under SU/SD. It was shown that under SU/SD conditions the large voltage windows and

high potentials occurring during cycle B (0.6–1.4 V) contribute most to the degradation of the present catalyst, while the narrow potential window applied during cycle C (1.0–1.4 V) in fact lowers the overall degradation. It was also shown that in the proposed *ex situ* test carbon corrosion was very low, making it likely that this does not contribute significantly to the catalyst degradation under SU/SD conditions. Degradation of the present catalyst is initially, during the first 200 cycles, dominated by the irreversible dissolution of Pt, while for longer cycling Pt particle growth/agglomeration contributes increasingly to the catalyst degradation, expressed by the loss in ECSA. At the end of the test, after 1000 cycles, the latter process has become the predominant failure mode.

References

[1] D. Papageorgopoulos, U.S. DOE activities related to fuel cell durability, in: 2nd International Workshop on Degradation Issues of Fuel Cells, Thessaloniki, Greece, 2011.
[2] A. Nelson, Fuel Cell Requirements and Challenges for Automotive Production, Ulm Electrochemical Talks (UECT), Ulm, Germany, 2010.
[3] J. Aragane, T. Murahashi, T. Odaka, J. Electrochem. Soc. 135 (1988) 844–850.
[4] K.F. Blurton, H.R. Kunz, D.R. Rutt, Electrochim. Acta 23 (1978) 183–190.
[5] G.A. Gruver, R.F. Pascoe, H.R. Kunz, J. Electrochem. Soc. 127 (1980) 1219–1224.
[6] J.A.S. Bett, K. Kinoshita, P. Stonehart, J. Catal. 41 (1976) 124–133.
[7] A. Honji, T. Mori, K. Tamura, Y. Hishinuma, J. Electrochem. Soc. 135 (1988) 355–359.
[8] J.A.S. Bett, K. Kinoshita, P. Stonehart, J. Catal. 35 (1974) 307–316.
[9] K. Sasaki, M. Shao, R. Adzic, in: F.N. Büchi, M. Inaba, T.J. Schmidt (Eds.), Dissolution and Stabilization of Platinum in Oxygen Cathodes, in Polymer Electrolyte Fuel Cell Durability, Springer, New York, 2009, pp. 7–27.
[10] J. Marcinkoski, J.P. Kopasz, T.G. Benjamin, Int. J. Hydrogen Energy 33 (2008) 3894–3902.
[11] T.L. Payne, T.G. Benjamin, N.L. Garland, J.P. Kopasz, ECS Trans. 16 (2008) 1081–1092.
[12] J. Zhang, J. Zhang, in: J. Zhang (Ed.), PEM Fuel Cell Electrocatalysts and Catalyst Layers – Fundamentals and Applications, Springer, New York, 2008, pp. 965–1002.
[13] W. Gu, R.N. Carter, P.T. Yu, H.A. Gasteiger, ECS Trans. 11 (1) (2007) 963–973.
[14] S. Maass, F. Finsterwalder, G. Frank, R. Hartmann, C. Merten, J. Power Sources 176 (2008) 444–451.
[15] S. Kundu, M. Cimenti, S. Lee, D. Bessarabov, Membr. Technol. (2009) 7–10.
[16] N.L. Garland, T.G. Benjaminb, J.P. Kopasz, ECS Trans. 11 (2007) 923–931.
[17] R. Mukundan, G. James, J. Davey, D. Langlois, D. Torraco, W. Yoon, A.Z. Weber, R.L. Borup, ECS Trans. 41 (2011) 613–619.
[18] R. Borup, J. Meyers, B. Pivovar, Y.S. Kim, R. Mukundan, N. Garland, D. Myers, M. Wilson, F. Garzon, D. Wood, P. Zelenay, K. More, K. Stroh, T. Zawodzinski, J. Boncella, J.E. McGrath, M. Inaba, K. Miyatake, M. Hori, K. Ota, Z. Ogumi, S. Miyata, A. Nishikata, Z. Siroma, Y. Uchimoto, K. Yasuda, K. Kimijima, N. Iwashita, Chem. Rev. 107 (2007) 3904–3951.
[19] Y. Shao, R. Kou, J. Wang, J.H. Kwak, V. Viswanathan, Y. Wang, J. Liu, Y. Lin, ECS Trans. 16 (2008) 361–366.
[20] A. Ohma, K. Shinohara, A. Iiyama, T. Yoshida, A. Daimaru, ECS Trans. 41 (2011) 775–784.
[21] L.C. Colmenares, A. Wurth, Z. Jusys, R.J. Behm, J. Power Sources 190 (2009) 14–24.
[22] Z. Jusys, J. Kaiser, R.J. Behm, Phys. Chem. Chem. Phys. 3 (2001) 4650–4660.
[23] Z. Jusys, H. Massong, H. Baltruschat, J. Electrochem. Soc. 146 (1999) 1093–1098.
[24] Z. Jusys, T.J. Schmidt, L. Dubau, K. Lasch, L. Jörissen, J. Garche, R.J. Behm, J. Power Sources 105 (2002) 297–304.
[25] H. Baltruschat, in: A. Wieckowski (Ed.), Differential Electrochemical Mass Spectrometry as a Tool for Interfacial Studies in "Interfacial Electrochemistry", Marcel Dekker, Inc., New York, 1999 (Chapter 33).
[26] T.J. Schmidt, H.A. Gasteiger, G.D. Stäb, P.M. Urban, D.M. Kolb, R.J. Behm, J. Electrochem. Soc. 145 (1998) 2354–2358.
[27] T. Biegler, D.A.J. Rand, R. Woods, J. Electroanal. Chem. 29 (1971) 269–277.
[28] S.D. Knights, K.M. Colbow, J. St-Pierre, D.P. Wilkinson, J. Power Sources 127 (2004) 127–134.
[29] C.A. Reiser, L. Bregoli, T.W. Patterson, J.S. Yi, J.D. Yang, M.L. Perry, T.D. Jarvi, Electrochem. Solid-State Lett. 8 (2005) A273–A276.
[30] J.P. Meyers, R.M. Darling, J. Electrochem. Soc. 153 (2006) A1432–A1442.
[31] V.I. Birss, M. Chang, J. Segal, J. Electroanal. Chem. 355 (1993) 181–191.
[32] S. Rinaldo, J. Stumper, M. Eikerling, J. Phys. Chem. C 114 (2010) 5773–5785.
[33] M. Uchimura, S. Sugawara, Y. Suzuki, J. Zhang, S.S. Kocha, ECS Trans. 16 (2008) 225–234.
[34] E. Antolini, J. Mater. Sci. 38 (2003) 2995–3005.
[35] R.L. Borup, J.R. Davey, F.H. Garzon, D.L. Wood, M.A. Inbody, J. Power Sources 163 (2006) 76–81.
[36] A. Horky, K. Beverage, O. Polevaya, Y. Shi, in: Proceedings of the Fuel Cells Durability, first ed., Knowledge Press, Brookline MA, 2006, pp. 133–150.
[37] P.J. Ferreira, G.J. la O', Y. Shao-Horn, D. Morgan, R. Makharia, S. Kocha, H.A. Gasteiger, J. Electrochem. Soc. 152 (2005) A2256–A2271.
[38] Y. Shao-Horn, W.C. Sheng, S. Chen, P.J. Ferreira, E.F. Holby, D. Morgan, Top. Catal. 46 (2007) 285–305.
[39] R.L. Borup, J.R. Davey, F.H. Garzon, D.L. Wood, M.A. Inbody, in: Proceedings of the Fuel Cells Durability, first ed., Knowledge Press, Brookline MA, 2006, pp. 21–42.
[40] W. Li, M. Ruthkosky, M. Balogh, R. Makharia, S. Oh, in: Proceedings of the Fuel Cells Durability, first ed., Knowledge Press, Brookline MA, 2006, pp. 101–114.
[41] W. Schmittinger, A. Vahidi, J. Power Sources 180 (2008) 1–14.
[42] W. Bi, T.F. Fuller, J. Electrochem. Soc. 155 (2008) B215–B221.